FREEMAN, R. (1980). *Proc. R. Soc. London*, pp. 149–178.
GERMAIN, G., MAIN, P. & WOOLFSON, M. M. (1971). *Acta Cryst.* A**27**, 368–376.
HULL, W. E. (1982). *Two-Dimensional NMR*. Karlsruhe: Bruker.
International Tables for X-ray Crystallography (1974). Vol. IV. Birmingham: Kynoch Press. (Present distributor Kluwer Academic Publishers, Dordrecht.)
JOHNSON, C. K. (1976). *ORTEP*. Report ORNL-3794. Oak Ridge National Laboratory, Tennessee, USA.
KRAPCHO, A. P. (1976). *Synthesis*, pp. 425–444.
LE PERCHEC, P. (1986). *Janssen Chim. Acta*, **4**(3), 17.
MARTIN, G. J. & MARTIN, M. L. (1971). *Manuel de Résonance Magnétique Nucléaire*. Paris: Azoulay.
MARTIN, S. F. (1980). *Tetrahedron*, **36**, 419–461.
MEESE, C. O. & WALTER, W. (1985). *Magn. Reson. Chem.* **23**, 327–329.
MORRIS, G. A. (1986). *Magn. Reson. Chem.* **24**, 371–403.
SAINSBURY, M. (1984). *Comprehensive Heterocyclic Chemistry*, Vol. 3, edited by A. R. KATRITZKY & C. N. REES, pp. 995–1038. Oxford: Pergamon Press.
SCHMIDT, R. R. (1972). *Synthesis*, pp. 333–350.
SCHOMAKER, V. & TRUEBLOOD, K. N. (1968). *Acta Cryst.* B**24**, 63–76.
SHELDRICK, G. M. (1976). *SHELX*76. Program for crystal structure determination. Univ. of Cambridge, England.
STEWART, R. F., DAVIDSON, E. R. & SIMPSON, W. T. (1965). *J. Chem. Phys.* **42**, 3175–3187.
TRUEBLOOD, K. N. (1978). *Acta Cryst.* A**34**, 950–955.

Acta Cryst. (1989). B**45**, 283–290

Three-Dimensional Electron Diffraction Structure Analysis of Polyethylene

BY HENGLIANG HU AND DOUGLAS L. DORSET

Electron Diffraction Department, Medical Foundation of Buffalo, Inc., 73 High Street, Buffalo, New York 14203, *USA*

(*Received* 11 *August* 1988; *accepted* 11 *January* 1989)

Abstract

The electron diffraction patterns of four zones, (0**kl**), (**lkl**), (**hhl**) and (**k+l,k,l**), were obtained from polyethylene epitaxially crystallized on benzoic acid. During evaluation of the data it was shown that incoherent multiple scattering is the main cause of perturbations of reflection intensity, a fact consistent with electron microscopic observations of multilayer crystal morphology. After correction for incoherent scattering, a three-dimensional structural analysis confirmed that the epitaxial crystals have orthorhombic chain packing in the $0_\perp$ subcell, *i.e.* the space group *Pnam*. The analysis, which involved combining the data of epitaxially grown crystals with those of crystals grown from solution, gave an R factor of 0·207 for a setting angle of 46·7°. At a significance level of 0·05, the accepted range of the chain setting angles is 44·5–49·6°.

Introduction

Given the availability of microcrystalline samples, three-dimensional electron diffraction structure analysis would be an ideal way to obtain more accurate conformational characteristics of polymer chains. So far only a small number of polymer structures has been based on three-dimensional structural analysis with electron diffraction data. The problem is how to correct various zonal data and how to obtain a nearly complete set of normalized three-dimensional intensities, requirements for which, up to now, there is very little experience. Various zonal patterns come from different microcrystals, which may experience different perturbative effects, including beam-induced radiation damage, bend deformation, n-beam dynamical diffraction and incoherent multiple scattering. Which of these is the major factor often depends on the morphology of microcrystal growth.

The orthorhombic packing of polyethylene (PE) with space group *Pnam* was determined by Bunn (1939) by an X-ray diffraction study of PE fibres which was based on 25 unique intensity data, three of which were from overlapped reflections. Recent determinations of the PE crystal structure by electron diffraction of the (**hk**0) zone from solution-grown crystals have shown that the molecular packing in the microcrystalline state is also *Pnam* and the setting angle φ, *i.e.* the angle the chain zigzag makes with the b axis (see Fig. 1*a*), is about 42° (Dorset & Moss, 1983). Nevertheless, solution-crystallized samples provide incomplete information (Dorset, 1985), principally as a result of limited data resolution, but also because the data are restricted to a single zone. On epitaxial orientation, PE crystallizes on the (001) crystal faces of benzoic acid (BA) (Wittmann, Hodge & Lotz, 1983) to project a view onto the molecular chains. Nevertheless, in earlier studies of PE, electron diffraction patterns were ambiguous (Wittmann, Hodge & Lotz, 1983; Moss, Dorset, Wittmann & Lotz, 1985–1986) since the zonal patterns were contaminated with contributions from upper layers, *i.e.* some reflections from different zones overlapped, leading to incorrect measurement of the

0108-7681/89/030283-08$03.00

reflection intensities. Thus, in order to make epitaxially oriented specimens useful for structure analysis, some means must be found to produce more perfect crystals. Originally the electron diffraction patterns from untilted crystals contained two mixed zones, (0**kl**) and (**hkl**) (Moss, Dorset, Wittmann & Lotz, 1985–1986), identical to those depicted in an earlier paper (Wittmann, Hodge & Lotz, 1983). In order to facilitate three-dimensional analysis, we were interested in obtaining only single-zonal patterns from untilted and tilted crystals, and then combining these in order to accumulate a large enough data set. As will be shown in this paper, after improving the crystallization and then combining these zonal data with the data from solution-grown PE, a three-dimensional electron diffraction structural analysis can be carried out.

Materials and computational methods

Commercially available polyethylene from Scientific Polymer Products, Inc. (Ontario, NY), was prepared as a dilute *p*-xylene solution. The weight-average molecular weight M_w is 2306; the number-average M_n is 2015. After a few drops of the solution had been dried on mica sheets and benzoic acid added, epitaxial crystals on benzoic acid were obtained following the methodology of Wittmann, Hodge & Lotz (1983). The only change in the present procedure is that, before removing the grids from the substrate, the whole sample sandwich was annealed at 353 K for 30 min on a Mettler FP82 hot stage.

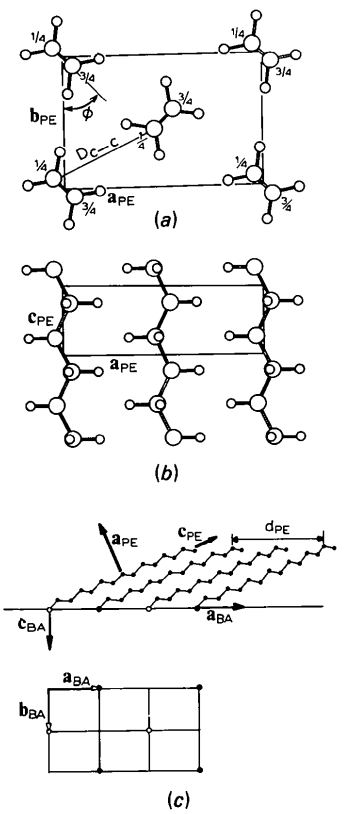

Fig. 1. Projection of PE 0_1 packing: (*a*) along the *c* axis and (*b*) along the *b* axis. (*c*) Projection scheme of a [10$\bar{1}$]-oriented PE crystal on the eutectic interface between PE and BA. Although the epitaxial relationship suggested in (*c*) implies an unfolded chain-end packing, the perturbations resulting from folds are unknown. Furthermore, the zone may also be caused by stable oblique chain packing.

Selected-area electron diffraction patterns obtained at room temperature (295 K) and at 100 kV with a Jeol JEM-100B electron microscope were recorded on Kodak DEF-5 X-ray film. Multiple recordings of the diffraction patterns at different exposure times ensured that all measured intensities were within the linear response of the film. As usual, precautions were taken to minimize radiation damage of the specimens (Dorset, 1985). The camera length was calibrated with a gold Debye–Scherrer diagram. Measurements of interpeak spacings on electron diffraction patterns were made with a film-reading device manufactured by Charles Supper, Inc.

Because of the arciform distribution of diffraction peaks, it was necessary to measure the integrated intensities. For this purpose, we employed different slit heights on a Joyce–Loebl MK III C microdensitometer and twice scanned each reflection spot in mutually perpendicular directions. The product of two peak-height intensities from different scans of a single reflection was used as the integrated intensity. No Lorentz correction was applied.

Structure factors $\mathbf{F}_{hkl}$ were computed in the usual way, *i.e.*

$$\mathbf{F}_{hkl} = \sum_j f'_j(\mathbf{s}_{hkl})\exp(i2\pi\mathbf{r}_j.\mathbf{s}_{hkl}) \qquad (1)$$

where f'_j is the Doyle–Turner (Doyle & Turner, 1968) electron form factor for atom j corrected for isotropic thermal motion, $\mathbf{r}_j$ is the atomic position in the unit cell and $\mathbf{s}_{hkl}$ is the reciprocal vector for reflection *hkl*. Some valence parameter values used in the computation are as follows: C–C bond length = 1·54 Å, C–H bond length = 1·06 Å, C–C–C spacing = 2·55 Å, ∠HCH = 109·47°. Isotropic thermal parameters used were: $B_C = 6{\cdot}0$, $B_H = 8{\cdot}0$ Å^2.

The Cowley–Moodie multislice formulation of dynamical diffraction theory was used to calculate the diffraction intensity data expected for *n*-beam dynamical scattering (Cowley & Moodie, 1957, 1959*a*,*b*; Goodman & Moodie, 1974) with the program *SHRLI* (O'Keefe & Buseck, 1979). Incoherent multiple scattering was modelled by the formula (Cowley, Rees & Spink, 1951):

$$K\mathbf{J}_{hk} = \mathbf{I}_{hk} + m_1\sum_{h_1}\sum_{k_1}\mathbf{I}_{h_1,k_1}\mathbf{I}_{h-h_1,k-k_1} + \ldots \qquad (2)$$

All multiple convolution products in (2) are ignored; we only consider the first and second terms on the right. $\mathbf{I}_{hk}$

represents the kinematical intensities, $\mathbf{J}_{hk}$ represents the total intensities from the crystal; K, m_1,... are constants which determine the relative contributions from various terms of the multiple scattering series in (2).

After correction for incoherent multiple scattering, several sets of intensity data, which come from different zones and are consistent with kinematical scattering, were obtained. Some reflections with the same indices might appear in several zones. A least-squares optimization was used for obtaining a set of three-dimensional data. For example, we have intensity data from different zones: $\{\mathbf{I}_{1j}\}$, $\{\mathbf{I}_{2j}\}$,... Let $\{\mathbf{I}_{0j}\}$ be a set of optimal three-dimensional data, which must satisfy the minimization of the following function (the destination function of the least-squares method):

$$S = \sum_j (K_1\mathbf{I}_{1j} - \mathbf{I}_{0j})^2 + \sum_j (K_2\mathbf{I}_{2j} - \mathbf{I}_{0j})^2 + \sum_j (K_3\mathbf{I}_{3j} - \mathbf{I}_{0j})^2 + \ldots \quad (3)$$

where the summation subscript j of the first term on the right encompasses all indices of the first zone, the j of the second term encompasses all indices of the second zone, and so on (*i.e.* each j represents a reflection index hkl). K_1, K_2, K_3, ... are normalized constants.

The usual crystallographic R factor

$$R = (\sum||F_{obs}| - k|F_{cal}||)/\sum|F_{cal}| \quad (4)$$

was used to estimate the fitting of the structure model to the observed data, where k is a scale factor such that $k\sum|F_{cal}| = \sum|F_{obs}|$.

Results and discussion

Figs. 1(*a*) and 1(*b*) depict the projections of polyethylene $0_\perp$ packing along the c and b axes, respectively, which are used in the model calculations. Three kinds of diffraction patterns were obtained from untilted specimens of epitaxial PE crystals (Figs. 2*a–c*). Obviously, Fig. 2(*c*) is the superposition of Figs. 2(*a*) and 2(*b*) and is identical to those obtained earlier (Wittmann, Hodge & Lotz, 1983; Moss, Dorset, Wittmann & Lotz, 1985–1986). The patterns as in Figs. 2(*a*) and 2(*b*) were obtained for the first time, taking advantage of the annealing process. From the positions of all the reflections, Figs. 2(*a*) and 2(*b*) correspond to (**0kl**) and (**hkl**) in single-zone patterns respectively (*cf.* Table 1). For [100] oriented crystals, corresponding to the (**0kl**) zone, the relative orientational relationship of polymer and substrate lattices is defined by $(100)_{PE} \parallel (001)_{BA}$ and $\mathbf{c}_{PE} \parallel \mathbf{a}_{BA}$. In this relationship, the lattice mismatchings amount to −3·9 and −8·0% in directions normal and parallel, respectively, to the PE chain axis (Wittmann, Hodge & Lotz, 1983). Even though these figures are well within accepted limits for epitaxy, the lattice mismatching certainly induces an increase in eutectic interface energy (Kerr & Lewis, 1971), the mismatching along

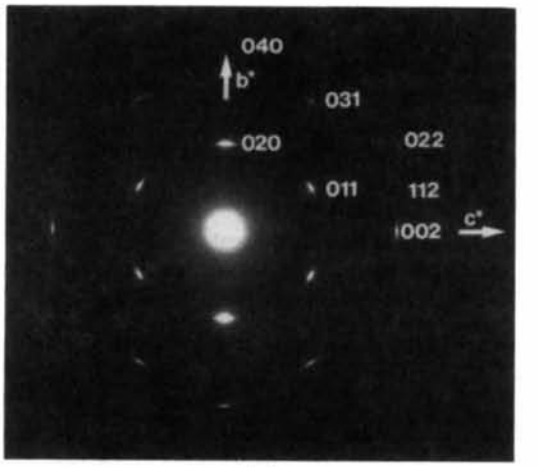

(*a*)

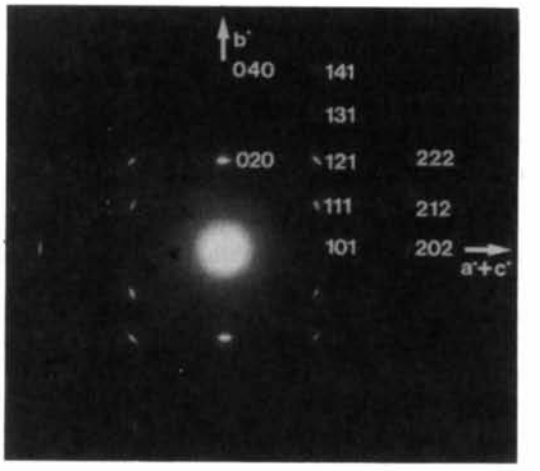

(*b*)

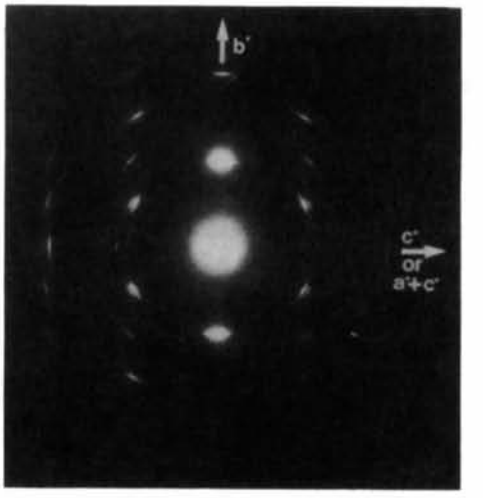

(*c*)

Fig. 2. (*a*) (**0kl**), (*b*) (**hkl**) and (*c*) mixed-zone diffraction patterns from an epitaxial PE crystal oriented on benzoic acid (BA). The crystals are untilted.

Table 1. *Unit-cell parameters* (Å, °): *comparison of observed and structure-model values*

Parameter	Model value	Observed value
c^*/b^*	1·9547	1·952 (10)
$\lvert\mathbf{a}^* + c^*\rvert/b^*$	2·0624	2·061 (10)
$c^*/\lvert\mathbf{a}^* + \mathbf{b}^*\rvert$	1·6330	1·623 (12)
$\lvert\mathbf{a}^* + \mathbf{c}^*\rvert/\lvert\mathbf{a}^* + \mathbf{b}^*\rvert$	1·7230	1·717 (12)
$\angle\mathbf{a}^* + \mathbf{b}^* \wedge \mathbf{a}^* + \mathbf{c}^*$	79·8	79·3 (3)

* Denotes a reciprocal parameter.

the **c** axis being somewhat larger. It is also possible to obtain [10$\bar{1}$] oriented crystals, corresponding to the (**lkl**) zone, on the eutectic interface. Fig. 1(*c*) shows a projection of the interface structure along the $\mathbf{b}_{PE}$ axis about [10$\bar{1}$] PE crystals. Utilizing the data: $a_{BA} = 5{\cdot}52$, $c_{PE} = 2{\cdot}55$, $a_{PE} = 7{\cdot}48$ Å, we found the spacing d_{PE} from Fig. 1(*c*) to be 10·86 Å. The lattice mismatching along the $\mathbf{a}_{BA}$ axis is $100[(d_{PE}-2a_{BA})/2a_{BA}] = -1{\cdot}6\%$. This value is smaller than −8·0% in the [100] PE epitaxial crystals. Therefore, the [10$\bar{1}$] orientation of PE crystals is reasonable from the viewpoint of spatial compatibility, although it may occur for other reasons such as a stable oblique packing of the polymethylene chains.

At a specimen tilt angle of 30–35°, two other kinds of diffraction patterns were obtained from epitaxial PE crystals on BA (Figs. 3*a*,*b*). The measurements of reflection positions (Table 1) indicate that the patterns of Figs. 3(*a*) and 3(*b*) are apparently only single-zone patterns, (**hhl**) and (**k+l,k,l**), respectively. Table 1 shows that there is very good agreement between the present experimental parameters and known parameters from the orthorhombic subcell of paraffin (Piesczek, Strobl & Malzahn, 1974). From our data we obtained the following unit-cell parameters:

$$a = 7{\cdot}48\ (2), \quad b = 4{\cdot}97\ (2), \quad c = 2{\cdot}55\ (1)\ \text{Å}. \quad (5)$$

On checking the diffraction patterns, we found that there are several extra reflection spots, which are forbidden by the space group, on the three patterns of zones (**lkl**), (**hhl**) and (**k+l,k,l**). On the (**0kl**) zone, there is an extra reflection near the 012 spot. From the position of this spot, we judged that it certainly does not belong to the (**0kl**) zone. As a result of lamellar twisting (Keith & Padden, 1959) or of progressive tilting of successive stacks of small lamellae (Bassett & Hodge, 1978), rotation of the **c** axis of the unit cell in the *ac* plane might be possible. As a consequence, the (112) plane would easily come into the diffraction position, in addition to the expected (**0kl**) patterns. From computation of the position and intensities, the appearance of this arced upper-layer (112) reflection is thus consistent with a simple rotation.

On the (**lkl**), (**hhl**) and (**k+l,k,l**) zone patterns there are extra (101, 010, 030), (001) and (101) reflection spots, respectively. By scrutinizing all the reflection spots in detail, we have found that almost every spot has an obvious arciform intensity distribution except these extra spots. Because the azimuthal distribution of the various arced reflections is different and since, therefore, the convolution products [equation (2)] would average over different arc orientations, the extra spots resulting from *n*-beam dynamical or incoherent multiple scattering should not be arced along a single azimuth (Fig. 4). This leads to a rule for judging whether or not certain spots are allowed by the space-group projections of the epitaxial PE crystals.

For further verification of perturbative errors in those four zones, intensity calculations for various crystal orientations would yield a more accurate determination than one based solely on lattice parameters. Although epitaxial crystals have a short projection axis to minimize crystal bend effects in terms of diffraction

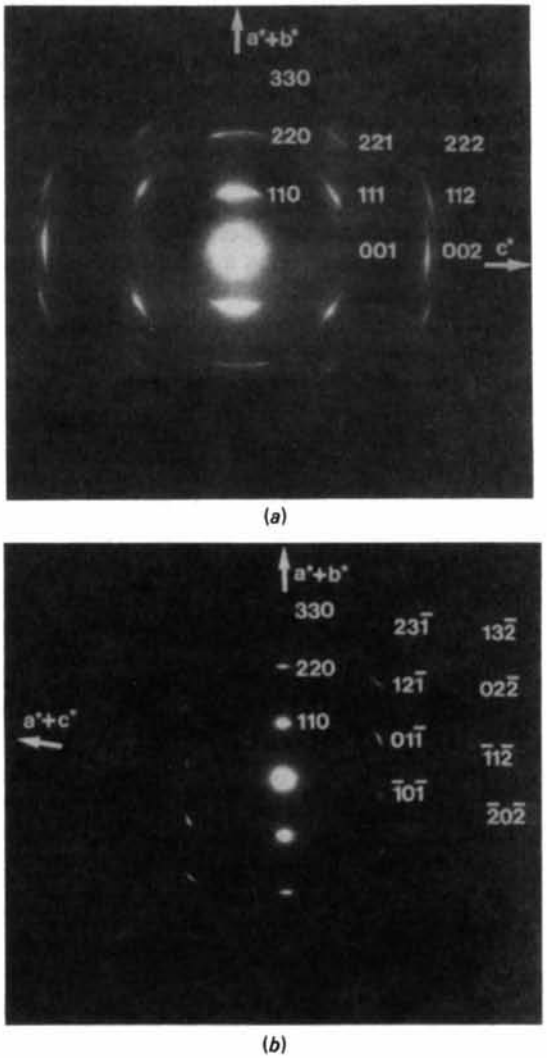

Fig. 3. (*a*) (**hhl**) and (*b*) (**k+l,k,l**) zone diffraction patterns from an epitaxial PE crystal on BA for crystals tilted 30–35°.

coherence (Cowley, 1961; Dorset, 1980), their irregular bend deformation (Moss, Dorset, Wittmann & Lotz, 1985–1986) might still influence the symmetry of reflection intensities. We utilized the average intensity of several symmetry-equivalent reflections as the observed intensity of those reflections for further calculation. All the *n*-beam dynamical scattering corrections of the four zones, on the other hand, did not produce any significant improvement in the residual *R* value, after using various crystal thicknesses in the model calculation.

For the incoherent multiple-scattering correction we were required to choose a starting structure model. Fortunately, the PE $0_\perp$ packing only has one adjustable parameter, *i.e.* the setting angle φ (see Fig. 1), while the unit-cell parameters were fixed as were the chain valence parameters (5). We chose $\varphi = 41{\cdot}3°$ as the starting setting angle. As was found for n-$C_{33}H_{68}$ (Dorset, 1986*a*), the electron diffraction data of epitaxial PE crystals for the (0**k**l) zone was closely matched to observed data without consideration of *n*-beam dynamical scattering and crystal-bending corrections. An *R* factor of 0·126 was obtained. The incoherent multiple scattering on the (0**k**l) zone also has little influence on the observed intensities (Hu, Dorset & Moss, 1988). For the (**hk**l) zone, the *R* factor before the incoherent-scatter correction was 0·339. After the incoherent-scatter correction, the *R*-factor was reduced to 0·178 (Table 2). This obviously showed that the incoherent multiple scattering is a major influence on reflection intensities in this projection. Because the crystal thickness is small enough, the *R* factors before and after the incoherent-scatter correction for the (**hh**l) zone are not very different; they are 0·137 and 0·131, respectively. A difference, similar to that found in the (**hk**l) zone, was observed for the (**k**+**l**,**k**,**l**) zone. The *R* factors before and after the incoherent-scatter correction were 0·255 and 0·179, respectively (Table 2). It should be reiterated here that similarly improved fits of observed and calculated data were not found when multislice dynamical calculations were carried out for all the zonal projections mentioned.

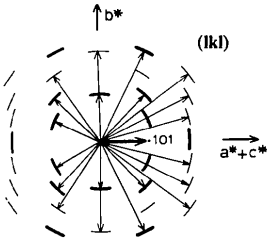

Fig. 4. Schematic pattern of the (**hk**l) zone. All Bragg reflections contributing to the (101) reflection in a convolution product are arced, as indicated by arrows with a radial distribution. From the convolution formula (2), a forbidden reflection such as (101) cannot have a specific arced distribution but will have a circular cross section.

Table 2. *Structure-factor comparison of observed diffraction data with calculated kinematical data* $|F_c|$ *and data* $|F_c'|$ *corrected for multiple scattering on the* (**hk**l), (**hk**0) *and* (**k**+**l**, **k**, **l**) *zone patterns*

h	*k*	*l*	$\lvert F_{obs}\rvert$	$\lvert F_{calc}\rvert$	$\lvert F_{calc}'\rvert$
(**hk**l)					
0	2	0	7·62	8·09	7·78
1	1	1	3·69	3·81	3·76
1	2	1	3·49	4·51	4·35
1	3	1	1·28	0·59	1·00
0	4	0	1·36	0·29	1·38
2	0	2	3·01	2·08	2·11
2	1	2	1·04	0·47	0·66
1	4	1	2·23	1·72	1·92
2	2	2	1·55	0·58	0·80
2	3	2	0·99	0·44	0·65
1	5	1	0·85	0·07	0·16
1	0	1	1·37	0·00	1·38
0	1	0	0·37	0·00	0·66
0	3	0	0·52	0·00	0·69
R factor				0·339	0·178
(**hk**0)					
1	1	0	8·33	9·17	7·98
2	0	0	6·76	8·73	7·71
2	1	0	2·22	1·91	1·77
0	2	0	4·15	3·96	4·67
1	2	0	1·99	1·51	1·64
3	1	0	3·25	2·49	3·96
2	2	0	3·19	1·49	3·19
4	0	0	2·60	2·67	3·31
3	2	0	2·09	1·45	1·60
4	1	0	1·96	1·02	1·25
1	3	0	1·84	1·20	1·89
2	3	0	2·16	1·17	1·30
4	2	0	1·55	0·45	1·26
5	1	0	1·77	0·84	1·52
3	3	0	1·48	0·39	0·90
5	2	0	1·84	0·81	1·02
6	0	0	1·06	0·51	1·15
4	3	0	1·99	0·73	1·01
6	1	0	1·06	0·51	0·69
6	2	0	0·89	0·06	0·46
5	3	0	1·12	0·20	0·38
6	3	0	1·00	0·45	0·61
7	2	0	1·06	0·35	0·52
R factor				0·344	0·210
(**k**+**l**,**k**,**l**)					
1	1	0	14·57	14·94	14·57
0	1	$\bar{1}$	5·35	5·56	5·48
2	2	0	3·41	2·44	3·46
2	1	1	1·27	3·26	3·21
1	2	$\bar{1}$	3·00	3·60	3·76
3	2	1	1·52	1·31	1·50
3	3	0	0·78	0·63	0·87
2	3	$\bar{1}$	1·32	1·41	1·64
$\bar{1}$	1	$\bar{2}$	2·19	1·70	1·73
2	0	2	2·03	1·66	1·70
0	2	$\bar{2}$	1·52	0·92	1·05
4	3	1	1·00	0·51	0·60
3	1	2	0·76	0·67	0·78
4	4	0	0·05	0·06	0·21
3	4	$\bar{1}$	0·95	0·61	0·70
1	3	$\bar{2}$	0·84	0·33	0·51
4	2	2	0·45	0·18	0·28
1	0	1	3·61	0·00	1·54
R factor				0·255	0·179

From the above corrections, the results showed that the epitaxially grown crystals might have a morphology with the following features: (*a*) a multilayer superstructure, with every layer thickness small enough so that there is no obvious intensity change from the *n*-beam dynamical scattering, (*b*) no strict regular packing between the layers of the same crystal and (*c*)

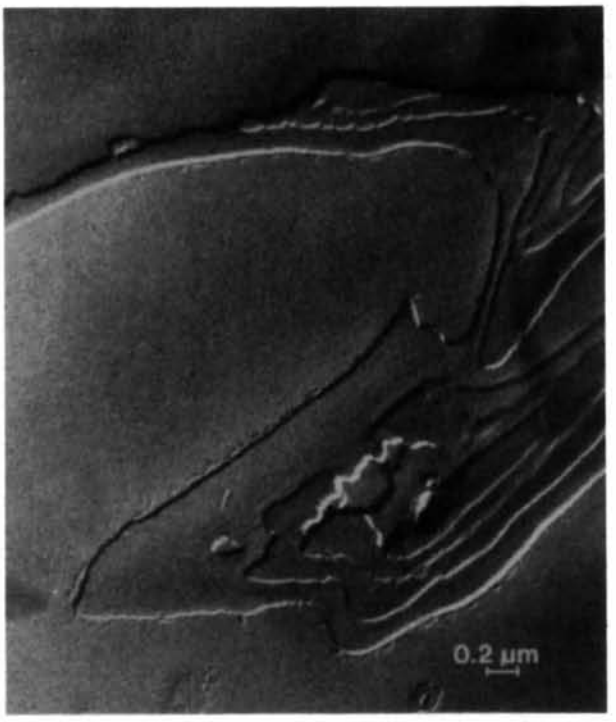

(*a*)

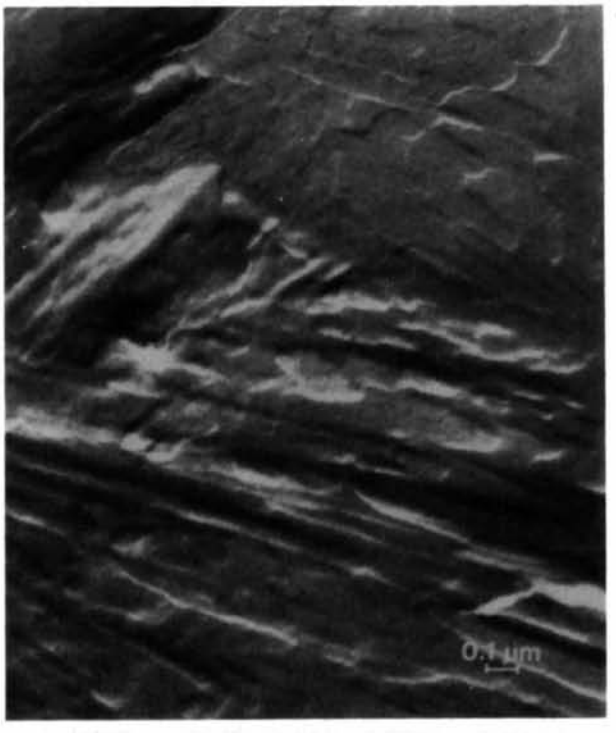

(*b*)

Fig. 5. Transmission electron image of a Pt–C-shadowed epitaxial PE crystal displaying (*a*) multilayer morphology and (*b*) disorientation between layers. (The contrast in these images is due to a fine coating of carbon–platinum evaporated *in vacuo* at an oblique angle to the crystal surface.)

only a small orientational difference between the layers, so that the arced reflection spots appear on the electron diffraction patterns. Figs. 5(*a*) and 5(*b*), which are electron microscopic images from epitaxial PE crystals on benzoic acid, demonstrate the multilayer structure and the orientation differences, respectively. (Before the images were taken, the crystals were finely coated with Pt–C at a small glancing angle.)

The agreement between observed and calculated data again indicates that the epitaxial PE crystals retain orthorhombic $0_\perp$ packing. For three-dimensional analysis, we utilized the process in (3) and then obtained a set of normalized three-dimensional intensity data from four sets of corrected zonal intensities assuming then that the kinematical model is correct. From this set of 34 reflection intensities, the setting angle φ and the R factor were computed as 43·6° and 0·189, respectively (Fig. 6*a*).

Based on the use of Hamilton's (1964) statistics, we evaluated the significance of the crystallographic R factor for a structural model in a refinement. The significance of an R-factor minimum for establishing the validity of an improved structural model within a confidence level α is based on the ratio $\mathscr{R} = R_1/R_0$, where R_1 and R_0 are the values for adjacent models.

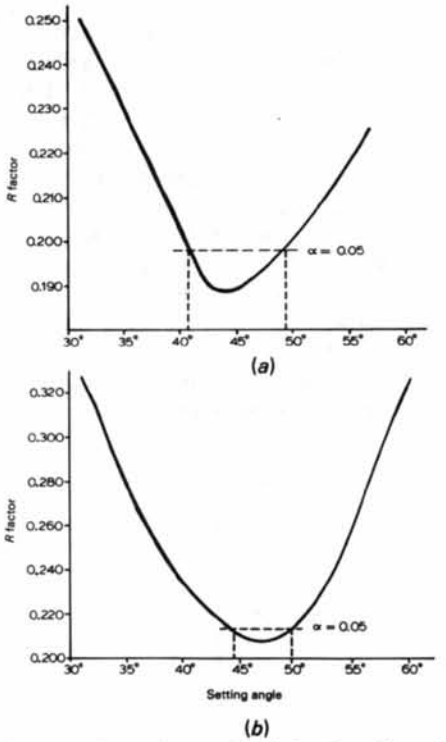

Fig. 6. R factor *vs* the setting angle: (*a*) for three-dimensional data obtained only from epitaxial crystals and (*b*) for a more complete data set, combining the (**hk**0) set obtained from solution-crystallized samples with that from the epitaxially oriented samples.

That is, if $\mathscr{R}$ exceeds a value $\mathscr{R}_{p,n-p,\alpha}$, then the hypothetical model R_1 can be rejected as being less satisfactory at the significance level α if $R_1 > R_0\mathscr{R}_{p,n-p,\alpha}$. For p refined parameters and n data the quantity is defined as

$$\mathscr{R}_{p,n-p,\alpha} = [\chi_p^2/(n-p) + 1]^{1/2} \quad (6)$$

where the values of χ_p^2 are from Table III of Hamilton (1964). In this study, $p = 1$ and $n-p = 33$; taking $\alpha = 0{\cdot}05$, $\mathscr{R}_{1,33,0.05} = 1{\cdot}057$. From Fig. 5(*a*) the acceptable range of setting angles φ is 40·5–49·5°. Compared with an earlier X-ray diffraction analysis (Kawaguchi, Ohara & Kobayashi, 1979), which had a setting-angle range 44–48° (Dorset, 1986*b*), even if our data set ($n = 34$) is larger than theirs ($n = 28$), the range of likely setting-angle values is still a little larger. Considering that we lack (**hk**0) zonal data, which are more sensitive to changes in chain orientation, the above result is reasonable.

A more complete set of three-dimensional data, which can be used for structural calculation, must therefore include some data which can sensitively reflect the change of the refinement parameters. Since we have verified the $0_\perp$ packing from epitaxial data, we can incorporate observed data from a solution-grown crystal (Dorset & Moss, 1983) with the same chain packing. Using our model, *i.e.* unit-cell parameters from (5) and a setting angle of 43·6°, the R factors before and after incoherent-scattering correction are 0·344 and 0·210, respectively (Table 2). The nearly complete set of three-dimensional data, which contains the combined solution and epitaxial crystal data, was again obtained by the process shown in (3). (Missing reflections in the final data set are due to the tilt limits of electron microscope goniometer stages – here ±60°.) The set contains 53 unique reflections, a more complete data set than used in all previous PE structural determinations. The setting angle φ and the R factor were computed as 46·7° and 0·207, respectively, from the nearly complete set of data (Table 3 and Fig. 6*b*). Using equation (6), $\mathscr{R}_{p,n-p,\alpha} = \mathscr{R}_{1,52,0.05} = 1{\cdot}036$. The acceptable range of the setting angle φ at $\alpha = 0{\cdot}05$ is 44·5–49·6° which is closer to the X-ray result, 44–48° (Dorset, 1986*b*). The setting-angle minimum is also closer to the result of the previous determination (in the X-ray case the minimum is 46°, as opposed to 46·7° found in our determination). Utilizing the derived structure model as a new starting model, we reapplied the incoherent-scattering correction of each zone to the refinement of a new three-dimensional data set which combined the solution and epitaxial data. Such an iteration process did not significantly improve the structure model.

Based on the acceptable setting-angle range, the shortest intermolecular distance D_{C-C} (Fig. 1*a*) between C atoms is 4·21 (1) Å, with the e.s.d. calculated from the φ range. Table 4 lists fractional coordinates of the unique atoms, with the e.s.d.'s also calculated from the φ range.

Table 3. *Structure-factor comparison of observed diffraction data with calculated kinematical data of the combined data set*

h	k	l	$\lvert F_{obs}\rvert$	$\lvert F_{calc}\rvert$	h	k	l	$\lvert F_{obs}\rvert$	$\lvert F_{calc}\rvert$
0	2	0	1·43	1·62	3	4	$\bar{1}$	0·21	0·13
0	4	0	0·27	0·13	1	3	$\bar{2}$	0·18	0·09
0	1	1	1·28	1·22	4	2	2	0·09	0·04
0	0	2	0·74	0·66	2	2	1	0·24	0·42
0	2	2	0·29	0·23	1	1	2	0·39	0·40
1	1	$\bar{1}$	0·62	0·78	3	3	1	0·19	0·13
2	0	2	0·54	0·37	3	3	2	0·03	0·03
2	2	2	0·21	0·11	2	0	0	2·88	3·10
1	1	0	3·55	3·47	2	1	0	0·91	0·89
2	2	0	0·56	0·57	1	2	0	0·69	0·53
3	3	0	0·19	0·13	3	1	0	0·77	0·84
0	6	0	0·15	0·05	4	0	0	0·79	0·78
0	3	1	0·57	0·57	3	2	0	0·71	0·58
0	5	1	0·13	0·14	4	1	0	0·60	0·54
0	4	2	0·00	0·02	1	3	0	0·44	0·52
1	2	1	0·68	0·78	2	3	0	0·73	0·42
1	3	1	0·20	0·16	4	2	0	0·21	0·17
2	1	2	0·19	0·10	5	1	0	0·37	0·23
1	4	1	0·41	0·31	5	2	0	0·56	0·32
2	3	2	0·18	0·08	6	0	0	0·18	0·04
1	5	1	0·17	0·01	4	3	0	0·54	0·28
2	1	1	0·29	0·70	6	1	0	0·29	0·23
3	2	$\bar{1}$	0·31	0·28	6	2	0	0·00	0·01
2	3	$\bar{1}$	0·23	0·32	5	3	0	0·24	0·06
4	3	1	0·22	0·10	6	3	0	0·27	0·15
3	1	2	0·15	0·14	7	2	0	0·27	0·12
4	4	0	0·05	0·02					
R factor									0·207

Table 4. *Atomic coordinates and e.s.d.'s* (Å)

	x	y	z
C	0·042 (2)	0·059 (3)	0·25
H1	0·181 (1)	0·023 (10)	0·25
H2	0·027 (8)	0·270 (2)	0·25

From the electron diffraction determination we have obtained some general rules for three-dimensional analysis. First of all, the crystal-growth technique must be improved to obtain undistorted zonal data. More zonal data from several orientations are helpful for increasing the validity of the structure model. After investigating crystal morphology, the major pertubation to the observed intensities should be found. After correcting intensities for multiple scattering, the least-squares method can then be used to obtain a three-dimensional set of reflection intensities. Finally, and most importantly, the set of data must include some reflections which are sensitive to the refined parameters, otherwise the precision of the final structure determination may not be good enough. The three-dimensional electron diffraction structure analysis reported here, therefore, is as accurate as the best powder X-ray diffraction study, although some uncertainty still remains in the precise determination of the chain setting angle.

The research described here was supported by a grant from the National Science Foundation (DMR

86-10783). We are grateful for advice from Drs J. C. Wittmann and B. Lotz concerning specimen preparation.

References

BASSETT, D. C. & HODGE, A. M. (1978). *Proc. R. Soc. London Ser. A*, **359**, 121–132.

BUNN, C. W. (1939). *Trans. Faraday Soc.* **35**, 482–491.

COWLEY, J. M. (1961). *Acta Cryst.* **14**, 920–927.

COWLEY, J. M. & MOODIE, A. F. (1957). *Acta Cryst.* **10**, 609–619.

COWLEY, J. M. & MOODIE, A. F. (1959*a*). *Acta Cryst.* **12**, 353–359.

COWLEY, J. M. & MOODIE, A. F. (1959*b*). *Acta Cryst.* **12**, 360–367.

COWLEY, J. M., REES, A. L. G. & SPINK, J. A. (1951). *Proc. Phys. Soc. London Sect. A*, **64**, 609–619.

DORSET, D. L. (1980). *Acta Cryst.* A**36**, 592–600.

DORSET, D. L. (1985). *J. Electron Microsc. Tech.* **2**, 89–128.

DORSET, D. L. (1986*a*). *J. Polym. Sci. Polym. Phys. Ed.* **24**, 79–87.

DORSET, D. L. (1986*b*). *Polymer*, **27**, 1349–1352.

DORSET, D. L. & MOSS, B. (1983). *Polymer*, **24**, 291–294.

DOYLE, P. A. & TURNER, P. S. (1968). *Acta Cryst.* A**24**, 390–397.

GOODMAN, P. & MOODIE, A. F. (1974). *Acta Cryst.* A**30**, 280–290.

HAMILTON, W. C. (1964). *Statistics in Physical Science*, p. 157. New York: Ronald Press.

HU, H., DORSET, D. L. & MOSS, B. (1988). *Ultramicroscopy*. In the press.

KAWAGUCHI, A., OHARA, M. & KOBAYASHI, K. (1979). *J. Macromol. Sci. Phys.* **16**, 193–212.

KEITH, H. D. & PADDEN, F. J. (1959). *J. Polym. Sci.* **39**, 101–123.

KERR, H. W. & LEWIS, M. H. (1971). *Advances in Epitaxy and Endotaxy*, edited by H. G. SCHNEIDER & V. RUTH, pp. 147–164. Leipzig: VEB Deutscher Verlag für Grundstoffindustrie.

MOSS, B., DORSET, D. L., WITTMANN, J. C. & LOTZ, B. (1985–1986). *J. Macromol. Sci. Phys.* **24**, 99–118.

O'KEEFE, M. A. & BUSECK, P. R. (1979). *Trans. Am. Crystallogr. Assoc.* **15**, 27–46.

PIESCZEK, W., STROBL, G. R. & MALZAHN, K. (1974). *Acta Cryst.* B**30**, 1278–1288.

WITTMANN, J. C., HODGE, A. M. & LOTZ, B. (1983). *J. Polym. Sci. Polym. Phys. Ed.* **21**, 2495–2509.

Acta Cryst. (1989). B**45**, 290–297

Charge Transfer and Three-Centre Bonding in Monoprotonated and Diprotonated 2,2′-Bipyridylium Decahydro-*closo*-decaborate(2−)

BY C. T. CHANTLER AND E. N. MASLEN

Crystallography Centre, University of Western Australia, Nedlands, Western Australia 6009, *Australia*

(*Received* 29 *September* 1987; *accepted* 16 *January* 1989)

Abstract

X-ray difference densities have been measured for the diprotonated form of the title compound at room temperature and for its monoprotonated analogue at 100 K. Atomic charges were determined by Hirshfeld's method of partitioning the difference density in proportion to atomic densities. Roughly 1·6 electrons are transferred to the $B_{10}H_{10}$ unit, and distributed widely over the cluster as a whole. That charge is less than the formal value of 2·0 electrons by an amount which correlates inversely with the strength of the interaction between the groups. The difference is not large, indicating that the cluster forms a robust, stable ionic species. Averaged difference densities in the B_3 rings resemble those reported by other workers. There is no evidence for open three-centre bonding. Closed three-centre bonds play a minor role in the redistribution of electron density. Asymmetric features in the difference maps are consistent with charge transfer resulting from close contact between B and N atoms. $C_{10}N_2H_{10}^{2+}.B_{10}H_{10}^{2-}$, $M_r = 276{\cdot}4$, monoclinic, $P2_1/c$, $a = 9{\cdot}937$ (4), $b = 10{\cdot}837$ (3), $c = 14{\cdot}856$ (5) Å, $\beta = 109{\cdot}21$ (3)°, $V = 1510{\cdot}6$ (9) Å^3, $Z = 4$, $D_x = 1{\cdot}22$ Mg m^{-3}, λ(Mo $K\alpha$) = 0·71069 Å, $\mu = 0{\cdot}0577$ mm^{-1}, $F(000) = 456$, $R = 0{\cdot}062$, $wR = 0{\cdot}047$ for 1771 observed reflections. $2C_{10}N_2H_9^+.B_{10}H_{10}^{2-}$, monoclinic, $P2_1/c$, $a = 11{\cdot}913$ (4), $b = 17{\cdot}656$ (5), $c = 11{\cdot}054$ (2) Å, $\beta = 101{\cdot}58$ (2)°, $V = 2278$ (2) Å^3, $Z = 4$, D_x 1·266 Mg m^{-3}, λ(Mo $K\alpha$) = 0·71069 Å, $\mu = 0{\cdot}0632$ mm^{-1}, $F(000) = 576$, $R = 0{\cdot}066$, $wR = 0{\cdot}045$ for 4524 observed reflections.

Introduction

Atomic charges can be determined from X-ray diffraction difference densities by the method of Hirshfeld (1977*a*,*b*). When applied to transition-metal complexes by Spadaccini (1988) and by Maslen, Ridout & Watson (1988), the results are remarkably consistent. The charges on individual atoms are smaller than the formal values, with magnitudes less than half an electron in most cases. On the other hand for polyatomic species such as hydrated metal ions the integrated charges are closer to the formal values. Consistent results were obtained even from diffraction experiments of structure determination quality, provided the data were not affected strongly by extinction (Maslen & Ridout, 1987).

If the error in the charge for a large molecular unit reflects the accumulation of uncorrelated uncertainties

0108-7681/89/030290-08$03.00